Journal of Infrared, Millimeter, and Terahertz Waves (2023) 44:1016–1037
https://doi.org/10.1007/s10762-023-00943-0

RESEARCH

Dual-Band (28/38 GHz) Compact MIMO Antenna System for Millimeter-Wave Applications

Rania R. Elsharkawy[1] · Khalid.F. A. Hussein[1] · Asmaa E. Farahat[2]

Received: 7 August 2023 / Accepted: 2 October 2023 / Published online: 18 October 2023

Abstract

The present work proposes a novel design of a dual-band-printed antenna for operation at the millimeter-wave frequencies 28 and 38 GHz that are utilized for the modern and future generations of mobile communications. The antenna is composed of two radiating elements. The first element is the main patch that is fed through a microstrip line with inset feed, and the second element is a parasitic element that is fed through capacitive coupling with the main patch. The design parameters of the proposed antenna are optimized through a complete parametric study to give excellent impedance matching at 28 GHz over the band 27.7–28.3 GHz and at 38 GHz over the band 37.7–38.3 GHz. The surface current distributions at the two operational frequencies are investigated. The designed antenna is used to construct a four-port efficient multi–input–multi–output (MIMO) system. The MIMO system performance is investigated regarding the envelope correlation coefficient (ECC), diversity gain (DG), and the channel capacity loss (CCL) showing very good performance. The single-element antenna and the MIMO are fabricated and experimentally evaluated showing excellent impedance matching over the lower and higher frequency bands, which come in agreement with the simulation results. It is shown that the antenna produces maximum gain of 7.4 and 8.1 dBi at 28 and 38 GHz, respectively. The average radiation efficiencies of the proposed antenna are 88% and 88.8% over the lower and higher frequency bands, respectively. In addition, the coupling coefficients between the MIMO antenna systems are measured experimentally showing very low coupling values resulting in an efficient MIMO system that is suitable for future millimeter-wave (mm-wave) applications.

Keywords MIMO · Printed antenna · Millimeter-wave

✉ Asmaa E. Farahat
e_asma_e@yahoo.com

Rania R. Elsharkawy
Raniarefaat85@yahoo.com

Khalid.F. A. Hussein
fkhalid@eri.sci.eg

[1] Microstrip Circuits Department, Electronics Research Institute (ERI), Cairo, Egypt

[2] Microwave Engineering Department, Electronics Research Institute (ERI), Cairo, Egypt

1 Introduction

The high demand for high-speed wireless communication has led to the development of millimeter-wave (mm-wave) frequency band (30–300 GHz) utilization. Among these bands, communication over the 28-GHz and 38-GHz spectra has garnered significant attention of researchers due to the wide bandwidth, fast data transmission, and low absorption rate [1]. The 28-GHz and 38-GHz frequency bands offer superior data rates and increased network capacity, making them ideal for 5G and beyond systems. The antennas working in these bands must be carefully designed to overcome challenges such as higher propagation losses and wider beam widths associated with mm-wave communications [2]. Additionally they must meet other requirements such as compact size, increased gain, and improved radiation patterns, while also ensuring efficient power transmission and reception.

Multiple-input-multiple-output (MIMO) antenna systems have led to the development of the communication systems. These systems depend on multiple antennas working simultaneously, to increase the capacity and allow high-speed data transmission. In addition, MIMO antenna systems provide several advantages such as spatial diversity and reduction of both fading and interference effects, thereby improving the reliability of wireless communications [3, 4]. MIMO antenna systems in the mm-wave band represent a key technology in 5G networks. Several antennas working at 28 GHz and 38 GHz have been introduced by researchers.

In Liu et al. [5], a multi-layer antenna structure based on a square patch radiator with a pair of shorting pins and an H-shaped slot achieves an impedance matching for 28-GHz and 38-GHz bands. The antenna is fed through a substrate-integrated waveguide (SIW) transmission line by means of a coupling slot. The antenna achieved gains of 9.0 dBi at 28 GHz and 5.9 dBi at 38 GHz. In Farahat et al. [6], an antenna based on a Yagi-Uda structure is presented. This antenna is used to operate at 28-/38-GHz bands. The antenna achieved gains of 9 and 10 dB at 28 GHz and 38 GHz, respectively. In Sehrai et al. [7], a tree-shape antenna structure operating from 23 to 40 GHz with dimensions of 40×40 mm is presented. A quad-port MIMO antenna with orthogonal element arrangement and dimensions of 80×80 mm is printed on an RT-5880 substrate with a loss tangent equal to 0.0009 and a relative permittivity of 2.2. The MIMO antenna system achieved a maximum total gain of 10.58, 8.87, and 11.45 dB, at 28 GHz, 33 GHz, and 38 GHz, respectively. The total efficiency of the antenna is 70%. In Halaoui et al. [8], an antenna with an inverted-F shape is presented to work at both frequency bands of 28 GHz and 38 GHz. The antenna is printed on FR4 substrate with dimensions of $5.5\ \text{mm} \times 4\ \text{mm} \times 0.2$ mm. An antenna array with 32 elements is deployed to achieve a gain of 16.52 dB at 28 GHz and 15.35 dB at 38 GHz. A dual-band antenna operating at 28 and 38 GHz is presented in Farahat et al. [9]. The design is mainly based on two coupled elements, primary and secondary elements. The primary antenna element is fed through a microstrip line, while the second element is capacitively coupled to the primary element. The antenna gain is about 6.6 dBi and 5.86 dBi at 28 and 38 GHz respectively. Two antenna elements are arranged side-by-side or front-to-front to establish a MIMO antenna. Khan et al.

[10] presented a wideband S-shaped four-port MIMO designed on RO5880 with bandwidth of 25–39 GHz. In Munir et al. [11], planar wideband multi-circular loop antenna mm-wave applications are introduced. The antenna has three circular rings with a partial ground plane with a square slot matched between 26.5 and 41 GHz, with a peak gain of 4 dBi and radiation efficiency of 96%. A four-element array system is designed with a total size of $18.25 \times 12.5 \times 0.254$ mm^3 and a peak gain of 11 dBi. An antenna with a vertically stacked dipole is introduced in [12]. It operates at two bands: 28 GHz and 38 GHz. The achieved gains are about 4.8 dBi and 4.6 dBi at 28 and 38.5 GHz, respectively. A wideband antenna that operates between 26.5 and 43.7 GHz is presented in Hussain et al. [13]. The antenna structure is based on a rectangular patch and a circular patch loaded with two stubs. Four antenna elements with orthogonal arrangement are used to get a MIMO antenna. The antenna gain is 8.4 dBi, and the channel capacity loss (CCL) is 0.001. In Raheel et al. [14], the authors introduce a dual-band antenna operating at 28 GHz and 38 GHz, simultaneously. Their antenna is simply based on a square patch with an E-shaped aperture and an H-shaped slot on it. Four antenna elements are arranged in an orthogonal order to constitute a MIMO antenna. The overall MIMO antenna dimensions are 20×24 mm and a gain of 7.9 dB is achieved.

The dielectric resonator (DR) is adopted to design a dual-band antenna [15]. A rectangular DR with a coplanar waveguide (CPW) feeder with cross and square slots is presented. A MIMO structure of two DR elements is established. The achieved diversity gain (DG), envelope correlation coefficient (ECC), and CCL are 9.98 dB, 0.007, and 0.06 bits/s/Hz, respectively. In Iqbal et al. [16], a single-fed dual-band circular polarized DR antenna is presented for dual-function communication, such as GPS and WLAN. The design achieved wideband impedance bandwidths of 6.4% and 25.26% and 3-dB axial ratios (ARs) of 21.26% and 27.82%, for the upper and lower bands, respectively. In Tadesse et al. [17], an antenna with a rectangular shape and an additional split-ring resonator unit cell are incorporated to resonate at 28 and 38 GHz. A MIMO antenna with quad ports is printed on Rogers RT5880 substrate with dimensions of $14 \times 14 \times 0.8$ mm. The antenna achieved an ECC less than 0.005, a DG close to 10 dB, and a CCL less than 0.35 bits/s/Hz. An antenna with a circular patch structure with additional rectangular slot is used to operate at 38 GHz [18]. The antenna bandwidth ranges from 36.6 to 39.5 GHz. A quad-port MIMO antenna with dimensions of $25.95 \times 25.95 \times 0.238$ mm^3 is designed to work at frequencies from 37.2 to 39.2 GHz. The MIMO antenna satisfies an isolation of less than 25 dB. The antenna peak gain is close to 10 dBi; this is due to using a large-frequency selective surface (FSS) layer below the MIMO antenna. The ECC and DG values are < 0.005 and around 9.99, respectively.

One of the primary challenges associated with MIMO antenna systems is the antenna coupling, which can lead to interference between the closely spaced antenna elements and, consequently, degradation of signal quality, increase of interference, and reduction of channel capacity [19]. The isolation between MIMO system elements is an important issue. It is needed to be high to minimize the coupling between the MIMO system elements and consequently enhance the overall performance. Coupling reduction methods in MIMO

antennas have been extensively studied in recent research works. Several techniques have been presented to minimize mutual coupling between adjacent antenna elements. Among these methods, band-pass filter (BPF) is used to select a desired band [20]. Electromagnetic band-gap (EBG) [21–23], stub [24], microstrip resonator [25], meander-line [26], neutralization line [27], shorting pin [28], and metasurfaces [29] are used in the antenna design.

The present work depends on a composite antenna structure with a primary and a coupled parasitic patch. This antenna structure supports the operation at 28-GHz and 38-GHz bands. Both the main patch and the parasitic element cooperate to allow the radiation at 28GHz. The main patch alone allows the radiation at 38 GHz. The antenna parameters are optimized to get an optimal antenna design considering the impedance bandwidth, gain, and efficiency. A quad-port MIMO antenna system with orthogonal antenna elements arrangement is established. The performance of the single antenna as well as the MIMO system is investigated and compared with other published work.

The paper is organized as follows. Section 2 presents the single element of the proposed dual-band antenna design. Section 3 describes the proposed MIMO system configuration. Section 4 illustrates the single-element antenna performance and the MIMO system characteristics. The fabrication and experimental work are investigated in Sect. 5. A comparison between the proposed antenna and the MIMO system is presented in Sect. 6. Finally, the conclusions of the work is summarized in Sect. 7.

2 Design of the Single-Element Dual-Band Antenna

In this section, the geometrical structure of the proposed single-element 28-/38-GHz antenna is illustrated and the optimum design parameters are selected.

2.1 Geometry Description

The antenna is first constructed from a circular patch with radius R_{P} as the main radiator according to the following equations [30]:

$$R_{\mathrm{P}} = \frac{F}{\left\{1 + \frac{2\mathrm{h}}{\pi\epsilon_{\mathrm{r}}F}\left[\ln\left(\frac{\pi F}{2h}\right) + 1.7726\right]\right\}^{1/2}} \tag{1}$$

$$F = \frac{8.791 \times 10^{9}}{f_{\mathrm{r}}\sqrt{\epsilon_{\mathrm{r}}}} \tag{2}$$

where ϵ_{r} and h are the substrate dielectric constant and substrate height, respectively.

Two side-ring extensions (with internal radius R_{E} and external radius R_{A}) have been attached to the main patch to add inductive loading to the main patch. Two

symmetric holes are included within these extensions. The radius of each hole is R_A. The main patch element is circularly clipped from the top. A crescent-shaped parasitic arc has been added to the antenna structure to add two types of loads to the main patch: first, a capacitive load through the semicircular slot of width W_S and, second, an inductive load as the crescent acts as semicircular turn of a coil, thereby adding an inductance effect to the antenna impedance. The crescent comprises a circular strip ring of outer radius R_o and inner radius R_i. Inside the circular ring, a circular patch exists. This circular patch is separated from the circular ring through a circular slot of width W_R to be coupled to each other. A small circular patch is placed at the center of this ring to be coupled to it through a circular slot of width W_R.

The main patch is fed through a microstrip line with an inset feed. This geometrical shape comprise the main patch, the inductive and capacitive loads, and the inset feed which provides a variety of dimensional parameters that enables the antenna designer to satisfy the antenna design goals at 28 GHz as well as 38 GHz.

The geometry of the proposed dual-band antenna is presented in Fig. 1. The antenna impedance is to be matched to 50Ω source over the desired frequency bands. The proposed patch antenna is printed on a Roger's RO3003 substrate of dielectric constant $\epsilon_r = 3$, loss tangent $\tan\delta = 0.001$, and thickness $h = 0.25$mm.

Another way to simplify the geometry description is to view the antenna as composed of two main radiating elements: the main patch and the parasitic element. The main patch is circular of radius R_P and has two side extensions. Each side extension

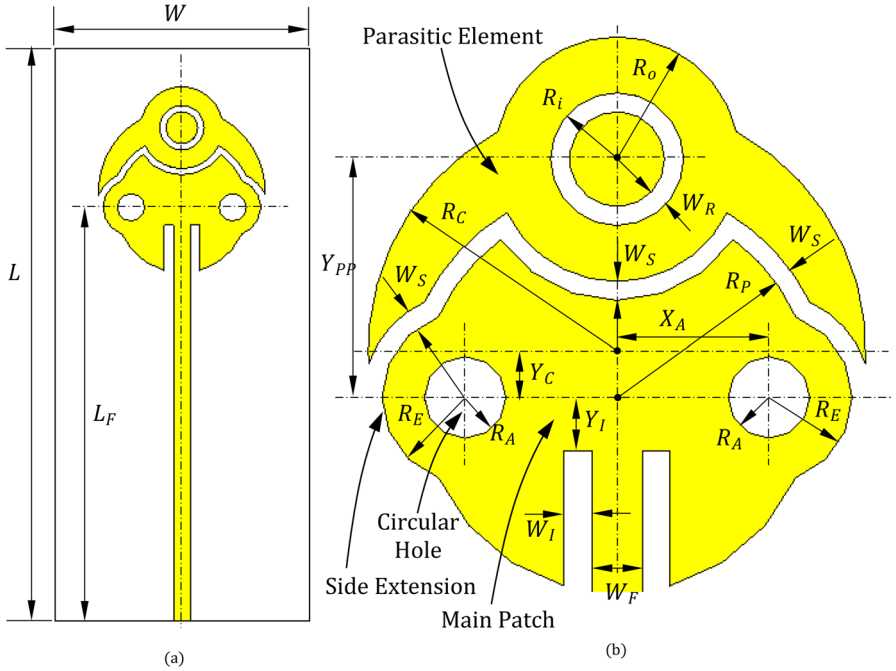

Fig. 1 Proposed dual-band antenna. **a** Feeding the antenna through microstrip line, **b** details of the radiating patch with the dimensional parameters

can be viewed as a small circular patch of radius R_E that is merged into the main patch and has a circular hole of radius R_A. The main patch is truncated at its upper part with a semicircular slot of width W_S to be coupled to the parasitic element. The parasitic element can be viewed as a crescent; a circular strip ring of outer radius R_o and inner radius R_i is merged into the crescent at its center. A small circular patch is placed at the center of this ring to be coupled to it through a circular slot of width W_R. The main patch is inset fed through a microstrip line. The inset length is L_I and the width of the side slots of the inset is W_I.

Such composite structure of the antenna allows the dual-band operation. The size of the overall surface of the main patch together with the parasitic element allows the formation of the resonant cavity field and the surface current that are responsible for radiation at the lower frequency (28 GHz). The surface of the main patch without the parasitic element allows the formation of the fields and surface currents of the resonant mode at 38 GHz. Thus, the resonance at 28 GHz is attributed to the existence of the two elements, namely, the main patch and the parasitic element, which allow radiation at 28 GHz. Both elements form a resonant cavity field at 28 GHz with a surface current that leads to radiation. On the other hand, the main element only allows a surface current that leads to radiation at 38 GHz. The geometrical design parameters shown in Fig. 1 are to be optimized through a complete parametric study to arrive at the final design with satisfactory performance regarding the impedance matching bandwidth, the gain, and the radiation efficiency.

The antenna has many curvatures that affect the antenna performance. The effects of these curvatures vary according to the role of each curved part. For example, the crescent subtending the main patch acts like a semicircular turn that adds inductive load on the main patch. The crescent curvature, R_C, controls the value of this inductive load, and, hence, it can be used to match the antenna input impedance to 50Ω and to increase its bandwidth at the lower and higher resonant frequencies. Also, the circular ring crossing the crescent has two radii describing its curvature: R_i and R_o. The two radii control the inductive coupling between the crescent and the main patch and play a major role in realizing the impedance matching at the higher resonant frequency (38 GHz). The curvature of the main patch itself has the radius R_P. This curvature has a major effect to set the resonant frequencies exactly at 28 GHz and 38 GHz.

Table 1 Dimensions of the proposed dual-band antenna design shown in Fig. 1

Parameter	L	L_F	R_P	R_C	R_E	R_A	R_o	R_i	W_I	W_R
Value (mm)	18	13	2.064	2.62	0.9	0.43	1.29	0.7	0.29	0.2
Parameter	W_S	W_F	W	X_A	Y_C	Y_I	Y_{PP}			
Value (mm)	0.2	0.53	8	1.6	0.5	0.565	2.0			

2.2 Optimum Design Dimensions

The final design dimensions of the proposed millimeter-wave antenna of the geometry presented in Fig. 1 are listed in Table 1. It should be noted that these dimensions are obtained through complete parametric studies to adjust the operating frequencies at 28GHz and 38GHz, to minimize the reflection coefficient at the antenna ports, and to maximize the gain and radiation efficiency over the two frequency bands. The study is made through numerical simulations using the commercial package CST®.

3 Proposed MIMO Antenna System Configuration

A compact four-port MIMO antenna system configuration with the dimension 26mm × 26mm is proposed for efficient MIMO operation. The system is constructed from four dual-band antennas arranged as shown in Fig. 2. Two antennas receive in the horizontal direction, and the other two antennas receive in the vertical directions. A square gap is created at the center of the MIMO circuit to reduce the mutual currents between the antennas. This allows reducing the coupling between the antenna elements and enhancing the MIMO performance at high bit rates. The MIMO parameters characterizing its performance are studied, including the coupling coefficients, envelope correlation coefficient, diversity gain, and radiation patterns. This MIMO system configuration is suitable for polarization diversity (as it has two vertical and two horizontal antennas that receive and transmit orthogonal polarizations) and spatial diversity (as the four antennas has four different spatial locations) schemes.

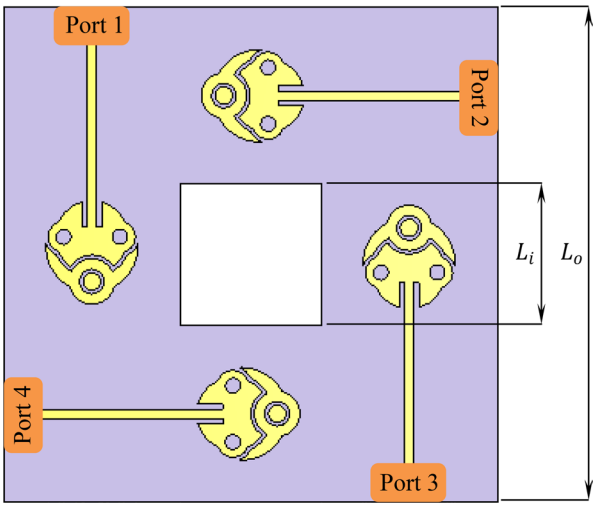

Fig. 2 Proposed four-port dual-band MIMO antenna system configuration

4 Results and Discussions

In this section, microwave electromagnetic simulations and experimental measurements are performed to investigate the single-element antenna performance as well as the proposed MIMO antenna system.

4.1 Single-Element Antenna Performance

The return loss, radiation pattern, gain, and efficiency of the single element are studied for the single antenna. Also the current distribution and the radiation mechanism are investigated in the following subsections.

4.1.1 Impedance Matching and Operating Bandwidth

The proposed antenna is designed on Rogers RO3003 with epsilon of 3, tangent loss of 0.002, and height of 0.25 mm. The patch antenna and the feeding microstrip line are made from high-conductivity copper. The antenna is simulated using the CST® electromagnetic simulator. Discrete port is attached between the microstrip line and the ground plane to form the feeding port. The resulting reflection coefficient is calculated numerically and shown in Fig. 3. It is found that the impedance is perfectly matched at 28 and 38 GHz with reflection coefficient of − 33 and − 51 dB, respectively.

4.1.2 Far-Field Patterns

The far-field radiation patterns are also calculated numerically using the CST® simulator at the two operating frequencies. The normalized patterns are plotted in Fig. 4a and b at 28 and 38 GHz, respectively, in the two principle planes $\phi = 0^{\circ}$ and $= 90^{\circ}$.

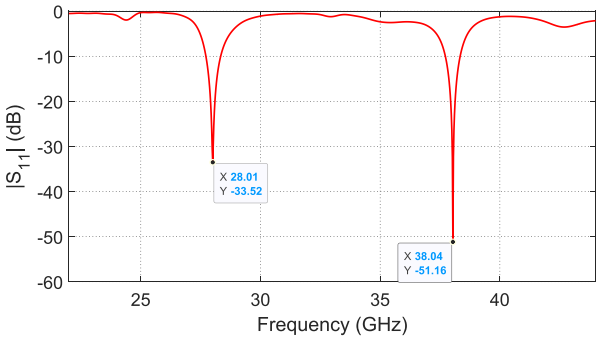

Fig. 3 Reflection coefficient of the proposed dual-band antenna

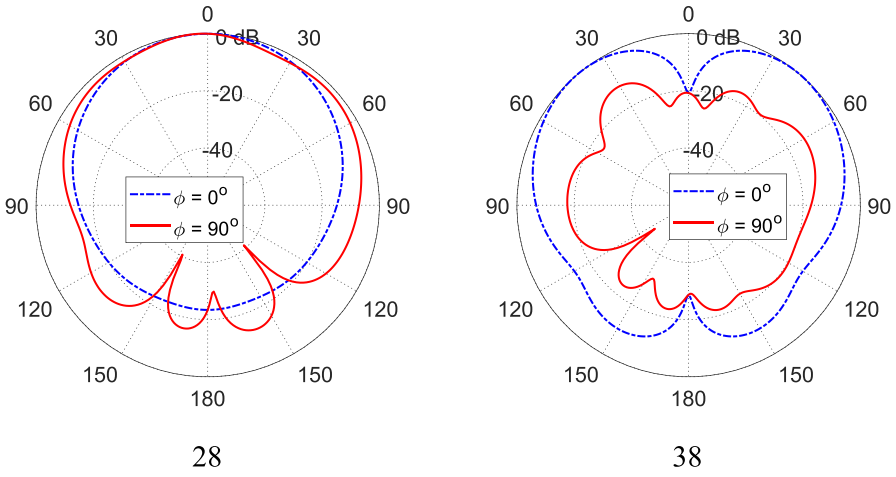

Fig. 4 Radiation pattern of the proposed dual-band antenna in the two principle planes $\phi = 0^{\circ}$ and $\phi = 90^{\circ}$, at **a** 28 GHz and **b** 38 GHz

4.1.3 Gain and Efficiency

The variations of the maximum antenna gain over the lower frequency band (27.7–28.3 GHz) and the higher frequency band (37.7–38.3 GHz) are presented in Fig. 5. It is shown that the maximum gain monotonically increases with increasing the frequency over the operational bands. However, the maximum gain obtained at 28 GHz reaches about 7.4 dBi, whereas the maximum gain obtained at 38 GHz is about 8.1 dBi. The values of the maximum gain with frequency are calculated

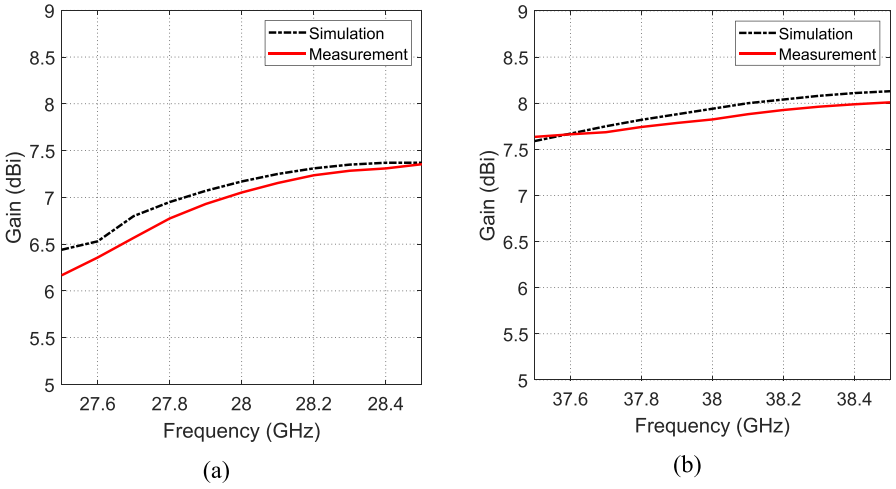

Fig. 5 Variation of the antenna gain over **a** the lower frequency band (27.7–28.3 GHz) **b** and higher frequency band (37.7–38.3 GHz)

numerically using the CST and is depicted in Fig. 5a and b for both operating frequency bands 28 and 38 GHz, respectively.

The variations of the total and radiation efficiencies of the proposed dual-band antenna over the lower frequency band (27.7–28.3 GHz) and higher frequency band (37.7–38.3 GHz) are presented in Fig. 6. It is clear that the average radiation efficiency is about 88% and the total efficiency is greater than 75% over the lower frequency band. On the other hand, the average radiation efficiency is about 88.8% and the total efficiency is greater than 77% over the higher frequency band.

4.1.4 Current Distribution and Radiation Mechanism

For understanding the mechanisms of radiation of the proposed dual-band antenna at 28 and 38 GHz, the patterns of the surface current on the main patch and the parasitic elements should be investigated. As shown in Fig. 7a, at 28 GHz, the surface current is concentrated on the main patch and is, also, extending through the coupling slot to flow with a significant magnitude on the parasitic element. Thus, both the main patch and the parasitic element contribute to the antenna impedance and the radiated field at 28 GHz. On the other hand, the surface current exists only on the main patch and on the edges of the coupling slot at 38 GHz as shown in Fig. 7b. The surface current does not flow on the parasitic element at this frequency. This means that the parasitic element affects only the antenna impedance at 38 GHz, but it has no contribution to the radiated field at this frequency.

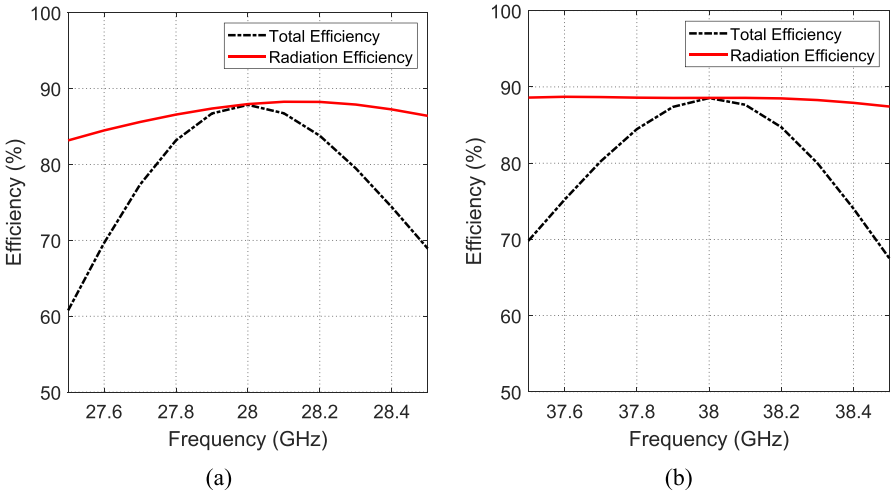

Fig. 6 Variation of the total and radiation efficiencies over **a** the lower frequency band (27.7–28.3 GHz) and **b** higher frequency band (37.7–38.3 GHz)

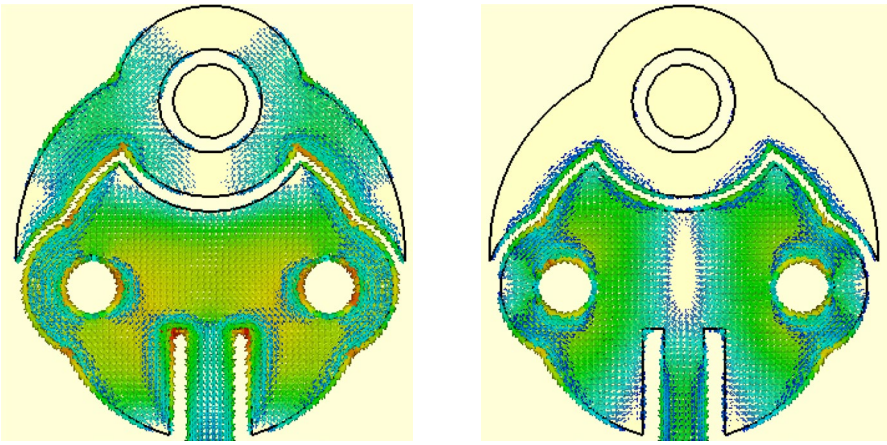

(a) (b)

Fig. 7 The current distribution on the surface of the antenna at **a** 28 GHz and **b** 38 GHz

4.2 Four-Port MIMO Antenna System Performance

The most important performance metrics for a MIMO system include the mutual coupling between antennas, the envelope correlation coefficient (ECC), the diversity gain (DG), the total active reflection coefficient (TARC), and the channel capacity loss (CCL). These measures are investigated in this section for the proposed dual-band MIMO system.

4.2.1 Impedance Matching and Coupling Coefficient

The self- and mutual-coupling between antennas are calculated through numerical simulations and plotted in Fig. 8. The mutual coupling is shown for the first antenna since the other antennas will have the same results as the MIMO configuration is

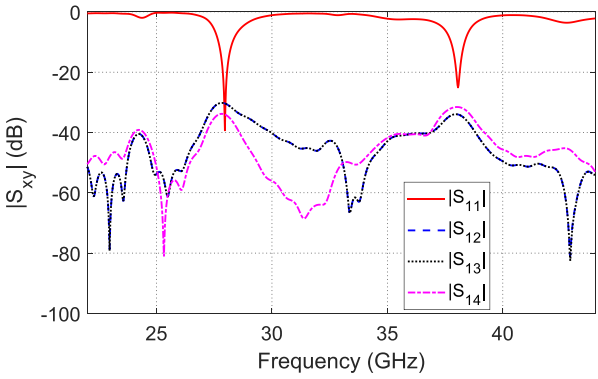

Fig. 8 Self- and mutual-coupling between MIMO antenna systems

reciprocal and all the antennas have the same positioning relative to the others. It is clear that the proposed arrangement causes the antennas to maintain very low coupling between each other and very good impedance matching at the operating frequencies 28/38 GHz. Figure 9 shows the current distribution on the four antenna surfaces when one antenna is excited. It is clear that the induced currents on the three antennas other than the excited one are very weak proving a very low mutual coupling.

4.2.2 Envelope Correlation Coefficient (ECC)

The ECC expresses how the radiation patterns of any two antennas in the MIMO system are independent. A low ECC value (preferred less than 0.5) indicates better signal quality, as it signifies independent channels with minimal interference and high capacity for data transmission. A high ECC means high correlated channels, leading to performance degradation. ECC is calculated according to the following formula [20]:

$$\mathrm{ECC} = \frac{\left|S_{11}^{*}S_{12} + S_{21}^{*}S_{22}\right|^{2}}{\left(1 - \left|S_{11}\right|^{2} + \left|S_{21}\right|^{2}\right)\left(1 - \left|S_{22}\right|^{2} + \left|S_{12}\right|^{2}\right)} \tag{3}$$

In Fig. 10, the ECC is plotted for each two pairs of antennas relative to antenna 1, (1, 2), (1, 3), and (1, 4). The other antennas 2, 3, and 4 will have the same results as antenna 1. From Fig. 10, we can see that the ECC value is almost zero at 28 and 38 GHz.

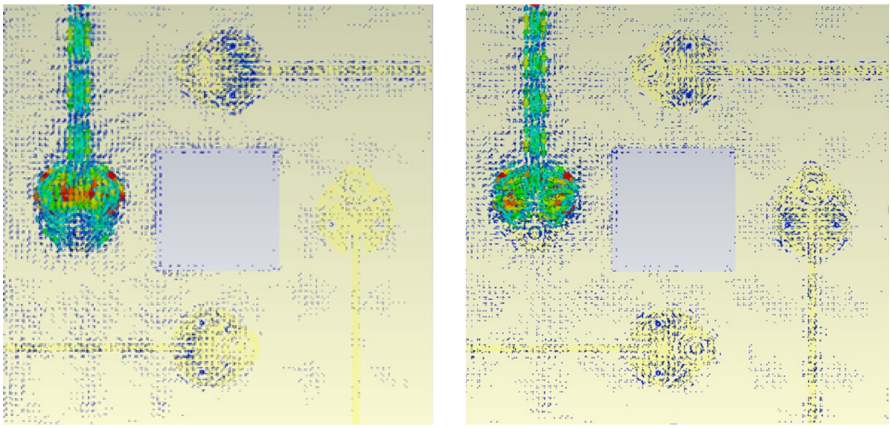

(a) (b)

Fig. 9 Current distribution on the four antennas of the MIMO system at **a** 28 GHz and **b** 38 GHz

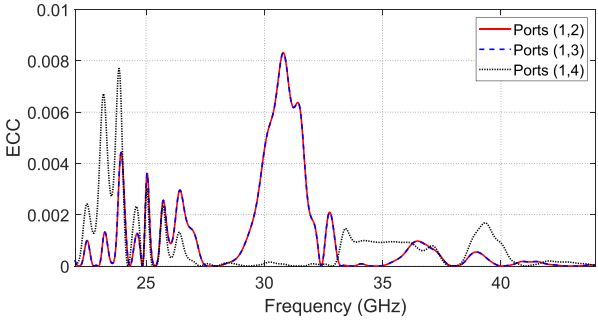

Fig. 10 Envelope correlation coefficient for the proposed four-port MIMO

4.2.3 Diversity Gain (DG)

Arranging the antennas for a MIMO system has a great effect on the signal to interference ratio according to the employed diversity scheme. This is measured through calculating the diversity gain (DG). It is an important factor for evaluation of the MIMO system performance. A higher value of DG means that the MIMO system effectively mitigates the adverse effect of the multipath propagation, leading to improved signal quality, higher data rate, extended coverage range, and enhanced overall system capacity. Thus, the transmitted power can be reduced without affecting the performance. It is calculated as follows [20]:

$$DG = 10 \times \sqrt{1 - ECC^2} \tag{4}$$

Figure 11 shows the variation of DG with frequency. It is shown that MIMO has a value greater than 9.99 at the 28 and 38 GHz bands.

4.2.4 Channel Capacity Loss (CCL)

Channel capacity loss (CCL) is an important parameter to evaluate the MIMO system performance in a multipath environment. It is estimated to define the upper limit of the data rate for reliable transmission in a communication channel. CCL of less than 0.3 bit/s/Hz is preferred. It can be calculated as follows [16]:

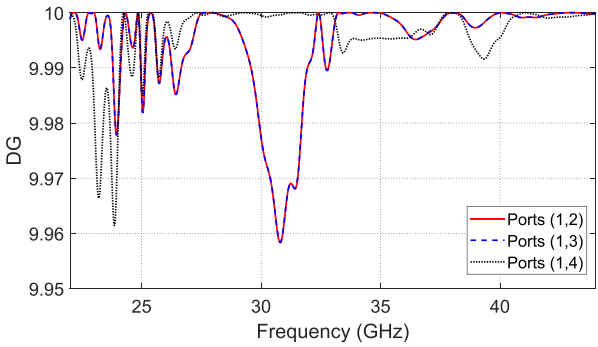

Fig. 11 Diversity gain for the proposed four-port MIMO system

$$\mathrm{CCL} = -\log_2 \det\left(\psi^{\mathrm{R}}\right) \tag{5}$$

where ψ^{R} is the correlation matrix that is calculated as:

$$\psi^{\mathrm{R}} = \begin{bmatrix} \rho_{11} & \rho_{12} & \rho_{13} & \rho_{14} \\ \rho_{21} & \rho_{22} & \rho_{23} & \rho_{24} \\ \rho_{31} & \rho_{32} & \rho_{33} & \rho_{34} \\ \rho_{41} & \rho_{42} & \rho_{43} & \rho_{44} \end{bmatrix} \tag{6}$$

$$\rho_{mm} = 1 - \left| \sum_{n=1}^{4} S_{mn}^{*} S_{nm} \right|, \rho_{mp} = - \left| \sum_{n=1}^{4} S_{mn}^{*} S_{np} \right|, m, p = 1, 2, 3 or 4 \tag{7}$$

The CCL is calculated and plotted against frequency in Fig. 12. It is shown that the proposed MIMO system has the best CCL (lowest) values at the 28-GHz and 38-GHz bands. CCL of 0.0064 is recorded.

4.2.5 Radiation Pattern

The far-field radiation pattern of the proposed MIMO antenna system is calculated through electromagnetic numerical simulation using the commercial package CST. In Fig. 13a and b, the simulated radiation patterns are drawn at 28 and 38 GHz, respectively, in the main planes $\phi = 0^{\circ}$ and $= 90^{\circ}$, when port 1 is excited. It is clear from the figure that the radiation pattern is not affected by the neighbor antennas (similar to the single element radiation pattern) because of the very week coupling between the antennas in the proposed MIMO configuration.

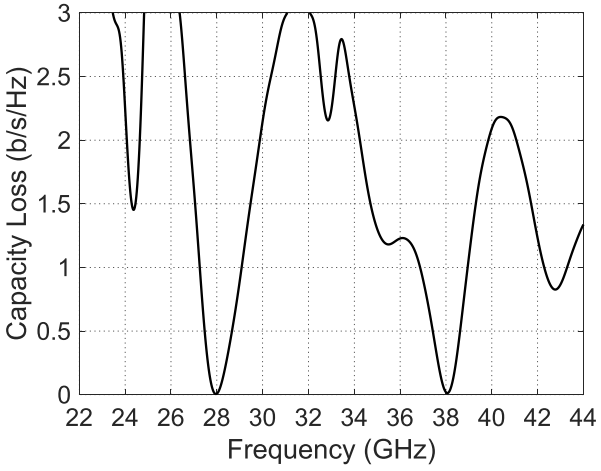

Fig. 12 CCL variation with frequency for the proposed MIMO system

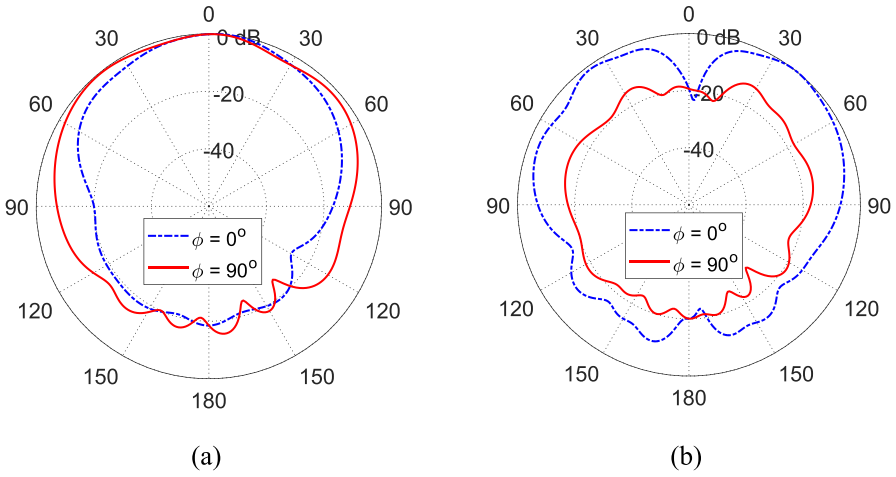

Fig. 13 Radiation pattern at **a** 28 GHz and **b** 38 GHz, in the two planes $\phi = 0^{\circ}$ and $= 90^{\circ}$

5 Fabrication and Measurements

In order to investigate practically the performance of the designed antenna with the dimensions listed in Table 1 and the constructed MIMO system, the proposed dual-band antenna is fabricated for this purpose on Rogers RO3003 with thickness of 0.25 mm. The four-port MIMO system shown in Fig. 2 is also fabricated on the same substrate. The fabricated antenna and MIMO system are subjected to experimental measurements and, its performance is compared to the simulation results. The fabricated models are shown in Fig. 14.

(a) The fabricated model of the dual-band antenna, (b) Fabricated MIMO antenna system.

Fig. 14 **a** The fabricated model of the dual-band antenna, **b** fabricated MIMO antenna system

5.1 Reflection Coefficient Measurement of the Single Element

The evaluation of the impedance matching of the proposed antenna is performed by measuring the reflection coefficient at the input port of the antenna. In order to measure the reflection coefficient using a vector network analyzer (VNA), an end-launcher connector is attached to the antenna as shown in Fig. 15a. The VNA ZVA67 is used for this function. The connection of the single antenna attached to the 2.4-mm end-launcher to the VNA is shown in Fig. 15b with the $|S_{11}|$ displayed on the screen. The measured reflection coefficient and the one calculated by the electromagnetic simulation are compared and plotted in Fig. 16 showing good consent.

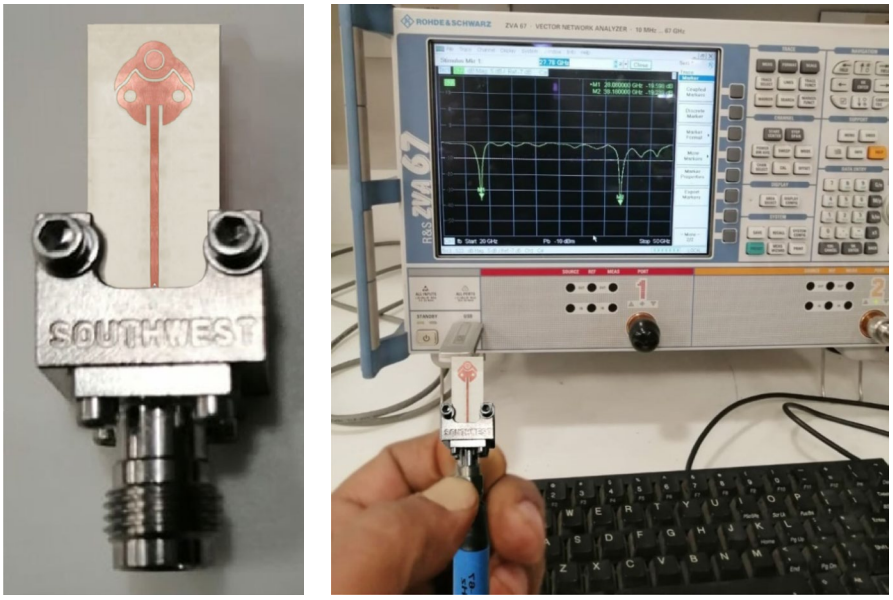

(a) (b)

Fig. 15 **a** Fabricated dual-band antenna attached to an end-launcher connector 2.4 mm from southwest microwave, **b** connection of the dual-band antenna to the VNA ZVA67

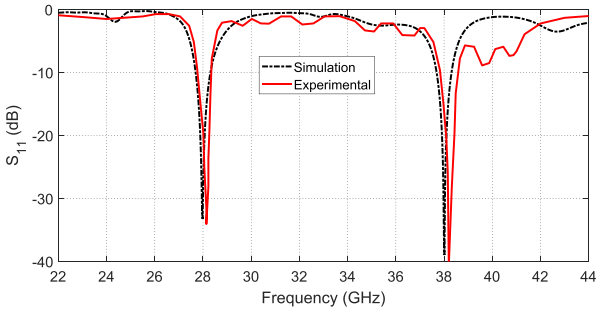

Fig. 16 Measured and simulated reflection coefficient of the proposed dual-band 28-/38-GHz antenna

5.2 Measurement of the Reflection and Coupling Coefficient of the MIMO Elements

The scattering parameters that are calculated in Fig. 8 are measured experimentally in this section. For the fabricated MIMO antenna system, the impedance matching for the four elements are measured practically using the VNA ZVA 67 from Rohde and Schwarz and plotted in Fig. 17. Also, the coupling coefficient between each two antennas is measured and illustrated in Fig. 18. It is clear that the coupling between the antennas is very weak, less than – 30 dB for all antenna couples.

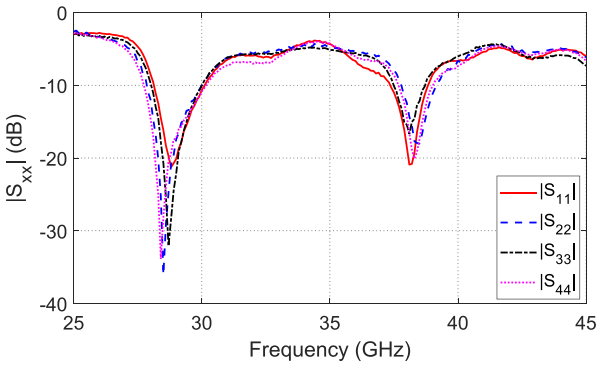

Fig. 17 Measured reflection coefficient of the four antennas of the proposed four-port MIMO

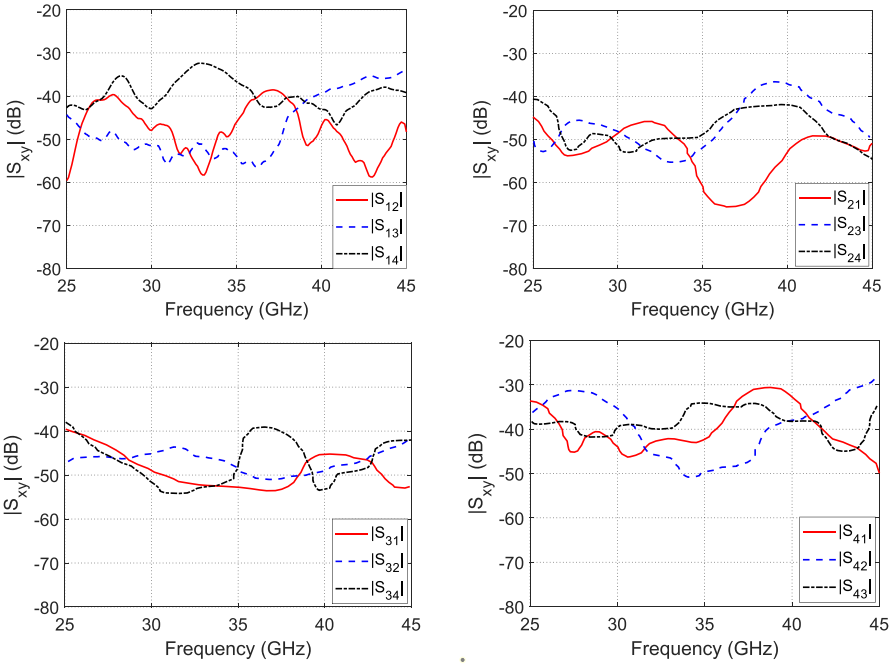

Fig. 18 Coupling coefficient between the antennas of the proposed MIMO system

5.3 Experimental Verification of the Far-Field Pattern of the Single Antenna

The far-field radiation pattern of the single-element antenna is measured experimentally using the same setup used in Fouad et al. [31], in the two principle planes. The measured patterns are compared to the ones calculated numerically using the CST in Fig. 19 showing good agreement.

The antenna maximum gain is measured experimentally as explained in Fouad et al. [31]. The measured gain is depicted in the Fig. 5 and compared with the simulated gain showing good agreement with the simulation results.

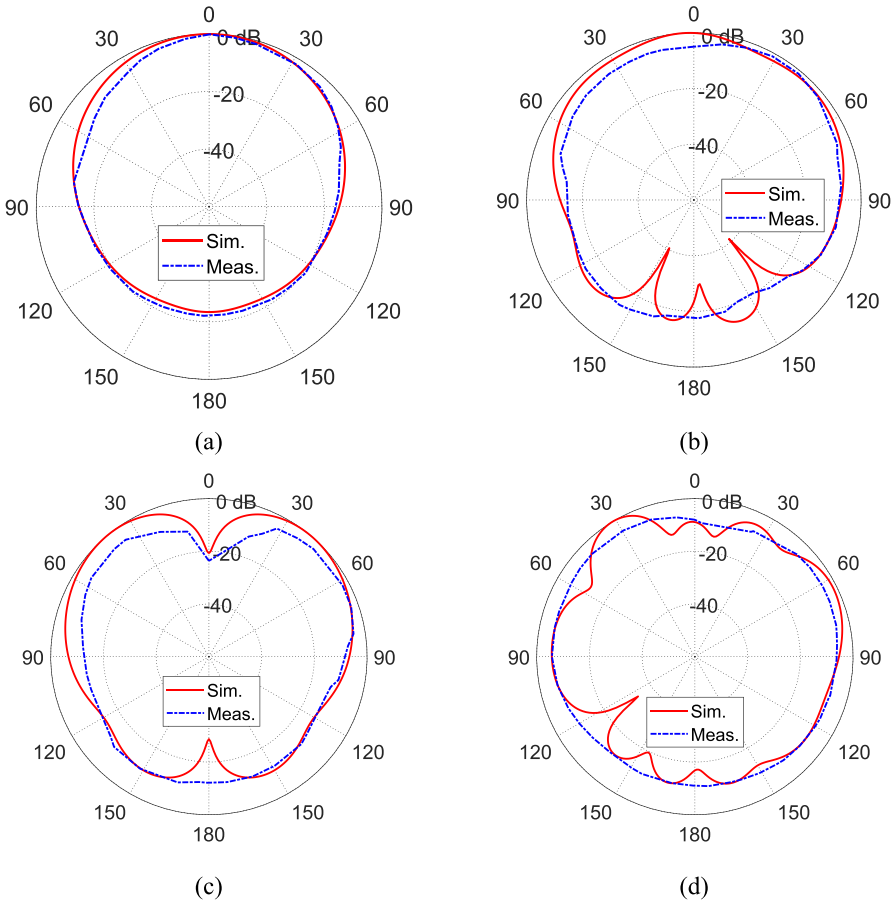

Fig. 19 Measured and simulated patterns of the far-field radiated by the dual-band antenna at 28 GHz in the planes a $\phi = 0°$ and b $\phi = 90°$, and at 38 GHz in the planes c $\phi = 0°$ and d $\phi = 90°$

6 Comparison between the Present MIMO Antenna System and the State-of-the-Art Work

The dimensions and some performance parameters of the dual-band (28/38GHz) antenna proposed in the present work are compared to those of other antennas of similar features presented in some recently published work. It is shown that the antenna proposed in the present work has the small size relative to those presented in Table 2. Also, the MIMO system is compared with other systems found in literature. The performance is compared from the point of view of number of operating bands, size, and isolation Table 3.

Table 2 Comparison between the present antenna design and the state-of-the-art work

Work	Dimensions (mm × mm × mm)	Bandwidth (GHz)		Maximum Gain (dBi)		Radiation Efficiency (%)	
		28 GHz	38 GHz	28 GHz	38 GHz	28 GHz	38 GHz
[9]	7.5 × 8.8 × 0.25	1.2	1.06	6.62	5.81	80	85
	20 × 20 × 1.57	4.8	3.6	5.75	7.23	NA	NA
[6]	21.6 × 20 × 0.25	3.42	1.45	9	8.8	98	96
[32]	20.4 × 26.4 × 0.5	0.7	12	7.03	7.3	86	96
[33]	10 × 10 × 0.254	0.5	0.7	7.4	8.1	77	91
	18 × 11.2 × 0.78	1.53	2.2	6.2	5.35	NA	NA
[Present]	4.95 × 5.80 × 0.25	0.6	0.6	7.37	8.13	88	88.6

Table 3 Comparison between the present MIMO antenna system and the state-of-the-art work

Work	No. of ports	Operating bands (GHz)	Size (mm×mm×mm)	Isolation (dB)
[34]	2	28	15×25×0.203	−30
[35]	4	28	30×35×0.76	−17
	2	28	33×27×0.76	−20
[36]	4	28/38	28×28×0.79	−30
[37]	4	28	30×30×1.575	−32
[17]	4	28/38	14×14×0.8	−22
[Present]	4	28/38	26×26×0.25	−33

7 Conclusion

A new design of a dual-band 28-/38-GHz-printed antenna is introduced that can be used for the millimeter-wave applications in the modern and future generations of mobile communications. The antenna is composed of two radiating elements. The first element is the main patch that is fed through a microstrip line with inset feed, and the second element is a parasitic element that is fed through capacitive coupling with the main patch. The design parameters of the proposed antenna are optimized through parametric study to give excellent impedance matching at 28 GHz over the band 27.7–28.3 GHz and at 38 GHz over the band 37.7–38.3 GHz. The surface current distributions at the two operational frequencies are investigated showing that the main patch is responsible for the radiation at the 28-GHz band, while the main and parasitic patches are responsible for the radiation at the 38-GHz band. The designed antenna is used to construct a four-port efficient MIMO system. The MIMO system performance is investigated regarding the envelope correlation coefficient (ECC), diversity gain (DG), and the channel capacity loss (CCL) showing very good performance. The ECC is about 0.0005 at both bands, the DG is less than 9.99, and the CCL is less than 0.0064. The single-element antenna and the MIMO are fabricated and experimentally evaluated showing excellent impedance matching over the lower and higher frequency bands, which come in agreement with the simulation results. It is shown that the antenna produces maximum gain of 7.4 and 8.1 dBi at 28 and 38 GHz, respectively. The average radiation efficiencies of the proposed antenna are 88% and 88.8% over the lower and higher frequency bands, respectively. Also, the coupling coefficients between the MIMO antenna systems are measured experimentally showing very low coupling resulting in efficient MIMO system for future millimeter-wave communications.

Funding Open access funding provided by The Science, Technology & Innovation Funding Authority (STDF) in cooperation with The Egyptian Knowledge Bank (EKB).

Data Availability Data sharing is not applicable in this article as no datasets were generated or analyzed during the current study.

Code Availability Not applicable; no codes were developed in this research.

Declarations

Conflict of Interest Authors declare that there are no Conflicts of interest/Competing interests for this research.

References

1. M. Hussain, E. M. Ali, S. M. R. Jarchavi, A. Zaidi, A. I. Najam, A. A. Alotaibi, A. Althobaiti, and S. S. Ghoneim, "Design and characterization of compact broadband antenna and its MIMO configuration for 28 GHz 5G applications," Electronics, Vol. 11, no. 4, 523, 2022.
2. S. Salous, V. D. Esposti, F. Fuschini, R. S. Thomae, R. Mueller, D. Dupleich, K. Haneda, J.M. Molina-Garcia-Pardo, J. Pascual-Garcia, D. P. Gaillot, M. Nekovee, S. Hur, "Millimeter-Wave Propagation: Characterization and modeling toward fifth-generation systems.[Wireless Corner].", *IEEE Antennas and Propagation Magazine, Vol.* 58, no. 6 pp. 115–127, 2016.
3. A. E. Farahat, and K. F. A. Hussein, "Dual-band (28/38 GHz) MIMO Antenna System for 5G Mobile Communications with Efficient DoA Estimation Algorithm in Noisy Channels", Applied Computational Electromagnetics Society Journal, Vol. 36, No. 3, pp. 282–294, 2021.
4. M. A. El-Hassan , A. E. Farahat, and Khalid. F. A. Hussein, "Quad-Band MIMO Antenna System for 5G Mobile Handsets", Applied Computational Electromagnetic Society (ACES) JOURNAL, Vol. 36, No. 11, November 2021.
5. P. Liu, X. Zhu ,Y. Zhang, X. Wang, C. Yang, and Z. H. Jiang, "Patch Antenna Loaded With Paired Shorting Pins and H-Shaped Slot for 28/38 GHz Dual-Band MIMO Applications," IEEE Access, Vol. 8, pp. 23705–23712, 2020.
6. A. E. Farahat, and K. F. A. Hussein, "28/38 GHz dual-band Yagi-Uda antenna with corrugated radiator and enhanced reflectors for 5G MIMO antenna systems", Progress In Electromagnetics Research C, vol. 101, pp. 159–172, 2020.
7. D. A. Sehrai, M. Abdullah, A. Altaf, S. H. Kiani, F. Muhammad, M. Tufail, M.Irfan, A. Glowacz , and S. Rahman, "A Novel High Gain Wideband MIMO Antenna for 5G Millimeter Wave Applications," Electronics, Vol. 9, No. 6, pp. 1-13, Jun. 2020.
8. M. El Halaoui, L. Canale, A. Asselman, and G. Zissis, "Dual-Band 28/38 GHz Inverted-F Array Antenna for Fifth Generation Mobile Applications," The 14th International Conference on Inter disciplinarily in Engineering—INTER-ENG 2020, Proceedings 63, no. 1: 53, 2020
9. A. E. Farahat, and K. F. A. Hussein, "Dual-band (28/38 GHz) wideband MIMO antenna for 5G mobile applications", IEEE Access, vol. 10, pp. 32213–32223, 2022.
10. M. A. Khan, A. G. Al Harbi, S.H. Kiani, A. N. Nordin, M. E. Munir, S. I. Saeed, J. Iqbal, E. M. Ali, M. Alibakhshikenari, and M. Dalarsson, "mmWave Four-element MIMO antenna for future 5G systems," Applied Sciences , Vol. 12, No. 9, p. 4280, 2022.
11. M. E. Munir, A. G. Al Harbi, S. H. Kiani, M. Marey, N. O. Parchin, J. Khan, H. Mostafa, J. Iqbal, M. A. Khan, C. Hwang, and R. A. Abd-Alhameed "A new mm-wave antenna array with wideband characteristics for next generation communication systems," Electronics Vol. 11, No. 10, p. 1560, 2022.
12. In-June Hwang, Ju-Ik Oh, Hye-Won Jo, Kwang-Seok Kim, Jong-Won Yu, Dong-Jin Lee, "28 GHz and 38 GHz Dual-Band Vertically Stacked Dipole Antennas on Flexible Liquid Crystal Polymer Substrates for Millimeter-Wave 5G Cellular Handsets " IEEE Transactions On Antennas and Propagation, Vol. 70, No. 5, pp. 3223–3236, May 2022.
13. S. A. Hussain , F. Taher , M. S. Alzaidi, I. Hussain , R.M. Ghoniem, M. Fathy, A. Sree ,and A. Lalbakhsh, "Wideband, High-Gain, and Compact Four-Port MIMO Antenna for Future 5G Devices Operating over Ka-Band Spectrum" Applied Sciences, Vol.13, No. 7, p. 4380, 2023.
14. K. Raheel , A. Altaf , A. Waheed, S. H. Kiani, D. A. Sehrai, F. Tubbal and R. Raad. " E-Shaped H-Slotted Dual Band mm Wave Antenna for 5G Technology" , Electronics, Vol. 10, 1019, 2021.
15. M. D. Alanazi, and S. K. Khamas, "A Compact Dual Band MIMO Dielectric Resonator Antenna with Improved Performance for mm-Wave Applications," Sensors vol. 22, 5056, 2022.
16. J. Iqbal, U. Illahi, M. A. Khan, A. Rauf, E. M. Ali, I. Bari, H. Ali, M. A. Khan, M. Alibakhshikenari, and M. Dalarsson, "A novel single-fed dual-band dual-circularly polarized dielectric resonator antenna for 5G Sub-6GHz applications," *Applied Sciences*, Vol. 12, no. 10, 5222, 2022.
17. A. D. Tadesse, O.P. Acharya, and S. Sahu "A Compact Planar Four-port MIMO Antenna for 28/38 GHz Millimeter-wave 5G Applications", Advanced Electromagnetics,Vol.11, No.3, pp.16–25, 2022.
18. Y. Richter, and I. Bergel, "Interference Effects on the MIMO Communications with Partial-Zero-Forcing Receivers", 2021 IEEE International Conference on Microwaves, Antennas, Communications and Electronic Systems (COMCAS), Tel Aviv, Israel, pp. 152–156, 2021.
19. A. A. Ibrahim, W. A. E. Ali, M. Alathbah, and A. R. Sabek, "Four-Port 38 GHz MIMO Antenna with High Gain and Isolation for 5GWireless Networks," Sensors, Vol. 23, 3557, 2023.

20. R. R. Elsharkawy, A. S. Abd El-Hameed, and S. M. El-Nady, "Quad-Port MIMO Filtenna With High Isolation Employing BPF With High Out-of-Band Rejection", IEEE ACCESS, Vol. 10, pp. 3814–3824, 2022.
21. M. B. Kadu, and N. Rayavarapu, "Compact stack EBG structure for enhanced isolation between stack patch antenna array elements for MIMO application," International Journal of Microwave and Wireless Technologies (Cambridge University Press), Vol. 13, No. 8, pp. 817–825, 2021.
22. A. Kumar, A. De, and R.K. Jain, "Novel H-shaped EBG in E-plane for Isolation Enhancement of Compact CPW-fed Two-Port UWB MIMO Antenna," IETE Journal of Research, pp. 1–7, 2021.
23. K. S. L. Parvathi, and S. R. Gupta, "Novel dual-band EBG structure to reduce mutual coupling of air gap based MIMO antenna for 5G application," AEU-International Journal of Electronics and Communications, Vol. 138, 153902, 2021.
24. A. H. Jabire, A.G. Abdullahi, S. Saminu, A. M. Jajere , A. M. Sadiq, "Mutual Coupling Reduction For Triple Band MIMO Antenna Using Stub Loading Technique," Sule Lamido University Journal of Science and Technology (SLUJST) , Vol. 2, No. 1, pp 53–64, 2021.
25. C. K. Ghosh1, M. Pratap1, R. Kumar1, S. Pratap, "Mutual Coupling Reduction of Microstrip MIMO Antenna Using Microstrip Resonator," Wireless Personal Communications, Vol. 112, No. 3, pp 2047–2056, 2020.
26. N. Kumar, and K. U. Kiran, "Meander-line electromagnetic bandgap structure for UWB MIMO antenna mutual coupling reduction in E-plane," AEU-Int. Journal of Electronics and Communication, Vol. 127, Art. No.153423, Dec. 2020.
27. K. V. Babu, and B. Anuradha, "Design of Wang shape neutralization line antenna to reduce the mutual coupling in MIMO antennas", Analog Integrated Circuits and Signal Processing (Springer US), Vol. 101, No. 1, pp 67–76, 2019.
28. M. Abdullah, Q. Li, W. Xue, G. Peng, Y. He, and X. Chen, "Isolation enhancement of MIMO antennas using shorting pins," Journal of Electromagnetic Waves and Applications, Vol. 33, No. 10, pp. 1249–1263, Jul. 2019.
29. H. Luan, Y. Wang, C. Chen and W. Chen, "Mutual Coupling Reduction of Closely E/H-coupled MIMO Antennas through Metasurfaces," 2019 International Symposium on Antennas and Propagation (ISAP), Xi'an, China, pp. 1–3, 2019.
30. Balanis, C.A. Antenna Theory: Analysis and Design, 4th ed.; John Wiley and Sons: Hoboken, NJ, USA, 2016.
31. Mohamed S. Fouad, Asmaa E. Farahat, Khalid F. A. Hussein, Abdel A. Shaalan, and Mai F. Ahmed, "Superwideband Fractal Antenna for Future Generations of Wireless Communication", Progress In Electromagnetics Research C (PIER C), Vol. 136, pp. 137–149, 2023.
32. F. Alnemr, M.F. Ahmed, and A. A. Shaalan, "A compact 28/38 GHz MIMO circularly polarized antenna for 5 G applications", Journal of Infrared, Millimeter, and Terahertz Waves, vol. 42, 338–355, 2021.
33. S. Chaudhary, and A. Kansal, "Compact high gain 28, 38 GHz antenna for 5G communication", International Journal of Electronics, vol. 110, no. 6, pp. 1028-1048, 2023.
34. H. Zahra, W. A. Awan, W. A. E. Ali, N. Hussain, S. M. Abbas, and S. Mukhopadhyay, "A 28 GHz Broadband Helical Inspired End-Fire Antenna and Its MIMO Configuration for 5G Pattern Diversity Applications," Electronics, Vol. 10, 405, 2021.
35. T. A. Balarajuswamy, and R. Nakkeeran, "Reconfigurable SIW antenna at 28/38 GHz for 5G applications", International Journal on Interactive Design and Manufacturing (IJIDeM), pp. 1-10, 2023.
36. M. Khalid, S. I. Naqvi, N. Hussain, M. Rahman, Fawad , S. S. Mirjavadi , M. J. Khan and Y. Amin, "4-Port MIMO Antenna with Defected Ground Structure for 5G Millimeter Wave Applications", Electronics, Vol. 9, p. 71, 2020.
37. M. Usman, E. Kobal, J. Nasir, Y. Zhu, Chao Yu, and A. Zhu, "Compact SIW Fed Dual-Port Single Element Annular Slot MIMO Antenna for 5G mmWave Applications" IEEE Access, Vol. 9, 2021.